Biocompatibility and Biodistribution of Surface-Enhanced Raman Scattering Nanoprobes in Zebrafish Embryos: *In vivo* and Multiplex Imaging

Yuling Wang,[†,‡,§] Jamie L. Seebald,[⊥] Daniel P. Szeto,[⊥] and Joseph Irudayaraj[†,‡,§,*]

[†]Bindley Biosciences Center, [‡]Birck Nanotechnology Center, [§]Agricultural and Biological Engineering, Purdue University, 225 S. University Street, West Lafayette, Indiana 47907, and [⊥]Department of Biological Science, Purdue University 915 W. State Street, Lilly Hall 2-218, West Lafayette, Indiana 47907

ABSTRACT Nanoparticles are increasingly being used to investigate biological processes in various animal models due to their versatile chemical, unique optical, and multifunctional properties. In this report we address the biocompatibility and biodistribution of nanoparticle sensors used for Raman chemical imaging in live zebrafish (Danio rerio) embryos. Surface-enhanced Raman scattering (SERS) nanoprobes (NPs) comprising gold nanoparticles (AuNPs) as enhancing substrate and nonfluorescent Raman labels were synthesized and microinjected into zebrafish embryos at the one-cell stage. Raman mapping was performed to assess their distribution in various cell-types and tissues of developing embryo at five different stages between 6 and 96 hpf (hours post-fertilization). Biocompatibility and toxicity studies indicate that the NPs are not toxic and the embryos were found to exhibit normal morphological and gene expression in addition to the proper form and function of major organs such as the heart and vasculature (of 7 day old NPs injected zebrafish embryos). A multiplex *in vivo* detection protocol was developed by SERS imaging to demonstrate that multiple labels can be detected by Raman mapping in undifferentiated cells as they develop into distinct cell- and tissue-types. The present work is the first to report on multiplex Raman imaging of zebrafish embryos with potential implications in tracking tissue development and biological processes at single molecule sensitivity using appropriate target molecules *in vivo*.

KEYWORDS: SERS nanoprobes · zebrafish embryos · multiplex *in vivo* Raman mapping · gene expression · biocompatibility · biodistribution

One of the key aspects in the formation of complex organs and tissues is to understand how and why progenitor cells are restricted to a particular developmental pathway due to the regulation of multiple signaling inputs. For example, skeletal muscle, blood, heart, bone, cartilage, and dermis of the vertebrate posterior body are derived from a small population of mesodermal progenitor cells that are spatially and temporally regulated due to the interplay of multiple signaling pathways that include bone morphogenetic proteins (Bmps),[1,2] Nodal,[3] and Wnts.[4−6] The advancement of cell-labeling techniques and imaging technologies provides an opportunity to track different cell-types in live embryos through space and time at subcellular resolution. Thus specification of the fate of the cells to form into different organs and tissues during development could be understood at the molecular scales.

Until now several imaging methods have been employed using nanoprobes (NPs) for *in vivo* studies including magnetic resonance imaging (MRI),[7] single photon emission computed tomography,[8] and dark-field[9] and fluorescence imaging,[10] to name a few. Surface-enhanced Raman scattering (SERS), has attracted much attention because of its ability to provide rich molecular information with high sensitivity due to the sharp and distinguishable vibration bands from the Raman spectra even under stringent physiological conditions.[11−13] The high sensitivity of SERS is due to the electromagnetic field coupling on roughened metal surfaces and junctions, which can cause the scattering signal of the molecule to increase by several orders of magnitude compared to fluorescence.[14−16] SERS detection is also considerably less sensitive to photobleaching and the characteristic Raman bands are up to 2 orders of magnitude narrower than fluorescence bands, which makes SERS imaging an exciting choice especially for the development of *in vivo* multiplex detection platforms.[17] Capitalizing on these unique features, recent studies have focused and reported on *in vivo* SERS imaging. For instance, dye molecules bound to gold nanoparticles (AuNPs) or silver nanoparticles (AgNPs) in living cells were shown to be trapped in the cytoplasm by SERS imaging.[18−24] Although a few previous studies have demonstrated the potential of SERS, the technology is still in its infancy and needs further refinement for use as a

*Address correspondence to josephi@purdue.edu.

Received for review October 18, 2009 and accepted June 07, 2010.

Published online June 16, 2010.
10.1021/nn100351h

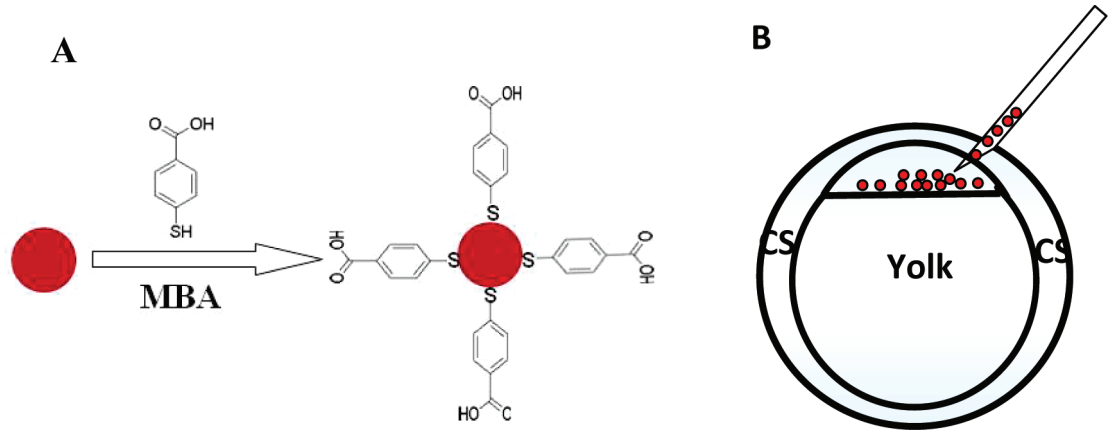

Scheme 1. Illustration of the SERS probe and the one-cell stage injection and not the yolk.

molecular imaging tool. More recent efforts have reported on the biocompatibility and localization dynamics of nanoparticles in zebrafish embryos.[25−27] However, their biodistribution in zebrafish embryos as cells develop into different organs after injection, starting from the one-cell stage, was not attempted. In addition, information on the choice of appropriate Raman labels and their toxicity is not available. The motivation thus is to demonstrate a Raman platform for multiplex chemical imaging of live zebrafish embryos.

Zebrafish was chosen as a model for sensor platform development because of its unique optical clarity, rapid growth and development, high fecundity, and availability of large numbers of genetic mutant zebrafish lines. Herein, we report the detection and imaging of microinjected SERS NPs *in vivo* in developing zebrafish embryos, from the one-cell stage. By SERS mapping we show their localization as the embryos develop into desirable stages as organs or tissues form and yet not affect the development from 4 h (40% epibobly stage) to 7 days post-fertilization.

Zebrafish embryos containing SERS NPs were evaluated using three different criteria: (1) molecular gene expression, (2) morphological formation of various tissues, and (3) physiological development. SERS *in vivo* imaging of zebrafish embryos during development shows that NPs appear to be spread throughout the cytoplasmic bridges that connect all zebrafish blastomeres. To the best of our knowledge, this is the first report on multiplex SERS imaging of zebrafish embryos to study its localization during development in conjunction with toxicity and gene expression studies. Our research can also be applied to track the fate of targeted NPs in dividing cells as they develop into tissues.

RESULTS AND DISCUSSION

Optimization of NPs and the Feasibility of SERS Detection in Zebrafish Embryos. Scheme 1 shows the composition of SERS probes and the injection process. Gold nanoparticles (AuNPs) were chosen as Raman label enhancers because of their ability to provide enhanced Raman scattering effects. The nonfluorescent molecule mercaptobenzoic acid (MBA) was chosen as one of the probes due to its unique and distinct vibrational bands. The conjugation of MBA on AuNPs was accomplished through the Au−S bond as shown in the left of Scheme 1. The injection was performed by direct delivery of NPs (Scheme 1A) into the cell region instead of the yolk at the one-cell stage (Scheme 1B). The ideal NPs for SERS detection in living subjects should have smaller dimensions (<60 nm), simple conjugation methods, minimum or no cytotoxicity, and provide ample enhancement for an intense and unique Raman spectra.[28] First, the size and concentration of nanoparticles were optimized to obtain a highly resolvable Raman spectrum at viable conditions from zebrafish embryos. Two different sizes of AuNPs (25 and 40 nm) were investigated, first in bulk solution and then in viable zebrafish embryos, respectively, as shown in Supporting Information Figure S1. The aromatic ring vibration bands, ν_{12} and ν_{8a} of MBA corresponding to 1078 and 1580 cm^{-1} were observed as expected.[29,30] Of the two sizes tested, AuNPs with the diameter of 40 nm yielded a higher enhancement both in solution (Supporting Information Figure S1A,a) and from live embryos (Supporting Information Figure S1B,a) and hence were used in further experiments. The morphology and optical properties of the optimized SERS NPs were then examined by TEM (Figure 1A) and UV−vis absorption spectra (Figure 1B). A slight red-shift in the surface plasmon resonance peak of AuNPs (curves a,b in Figure 1B) after modification by MBA confirms the functionalization step of MBA to AuNPs through the thiolated linkage.

Two different concentrations of AuNPs were used to further compare and optimize the signal as indicated in Supporting Information Figure S2. The concentration of AuNPs was calculated assuming that the gold in the $HAuCl_4$ was reduced and excess MBA molecules removed through centrifugation. As expected, a high concentration of AuNPs (5.0 nM) gave a much stronger SERS signal compared to samples with a lower (1.25 nM) concentration (Supporting Information

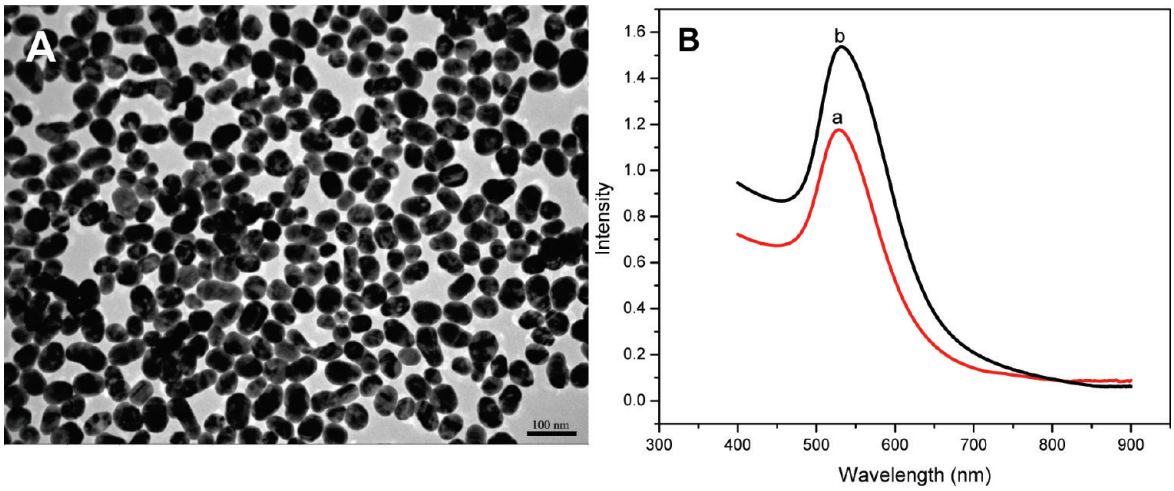

Figure 1. Typical TEM image of AuNPs (A) and UV−vis absorption spectra (B) of AuNPs (a) and AuNPs modified by MBA to constitute SERS nanoprobes (b).

Figure S2,a). Therefore, AuNPs at a concentration of 5.0 nM were chosen for *in vivo* SERS imaging experiments.

To more clearly demonstrate the feasibility of SERS mapping in zebrafish embryos, Raman spectra from early stage embryos were shown in Figure 2. Embryos at the 6−8 hpf (hours post fertilization) stage were first selected because at this stage different tissue and organ progenitor cells are specified (Supporting Information Scheme S1).[31] Subsequently, the distribution of SERS NPs in the different organs and tissues at later stages could be followed. The optical image of zebrafish embryo with a low resolution (4×) objective (Figure 2A) shows the ventral view of the embryo at 6−8 hpf. Inspection of embryo between 6 and 8 hpf revealed

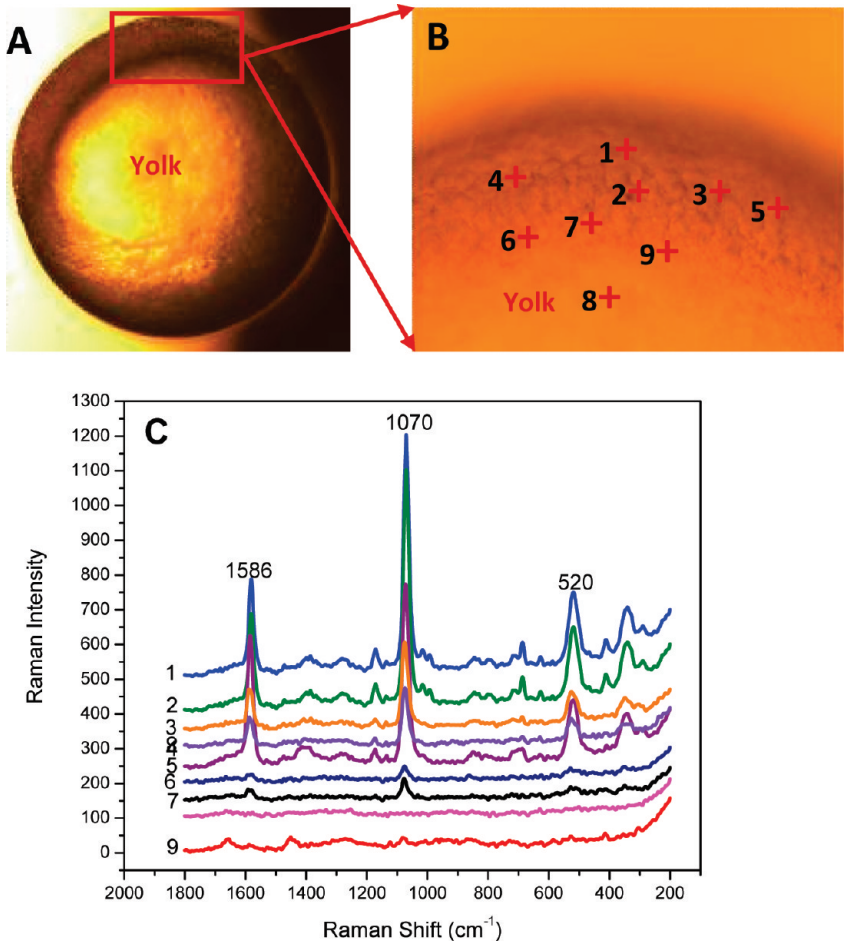

Figure 2. Optical image of zebrafish embryo at the early stage (6−8 hpf): (A) 4× and (B) 20× objective lens and (C) SERS spectra from zebrafish embryo at the indicated points in panel B .

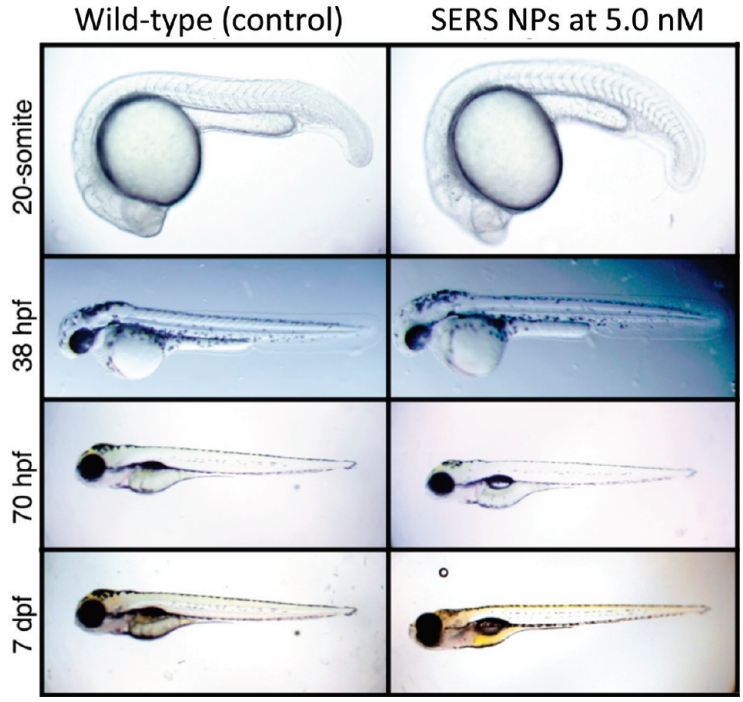

Figure 3. Microscopic images of wild-type embryo (left) and injection of 5 nM concentration of of SERS NPs (right).

that most of the SERS NPs were distributed almost non-uniformly in the mesodermal region of the embryo (in Supporting Information Scheme S1, the mesodermal region can be seen as a broad marginal zone) and no signal could be obtained within the yolk. Different spots were selected from the optical image of the projected section containing both the mesoderm and the yolk in Figure 1B for Raman spectra acquisition (Figure 2C). Even though the number of particles per cell decreased overtime after the initial injection into the one-cell stage of zebrafish embryos with approximately 3×10^6 particles, distinct SERS signal could be obtained from the selected section of the early embryo with high fidelity. Our observation suggests that SERS NPs are excellent sensors to study the distribution of NPs in zebrafish embryo.

Comparison of Morphological and Functional Development of Zebrafish Embryos Injected with SERS NPs. The toxicity of nanoparticles is an important concern in the development of a meaningful SERS platform for *in vivo* monitoring. Early studies illustrating the cytotoxicity of AuNPs and AuNPs conjugates have shown that the size, surface charge, or coatings on AuNPs will slightly influence their toxicity.[32−36] For example, Connor *et al.* reported that AuNPs coated by citrate or biotin show no apparent toxicity even at 250 μM to leukemia cells after exposure for 3 days, while cysteine or glucose coated AuNPs exhibited no cytotoxicity at a concentration of 25 μM to K562 cells even after 3 days of exposure.[37] However, similar research conducted in zebrafish embryos using silver nanoparticles (AgNPs) show an almost 100% mortality at 120 h post fertilization, while AuNPs had less than 3% mortality at the same time point.[38] Besides the toxicity of AuNPs and AgNPs,[26,38] nickel nanoparticles,[39] metal oxide nanoparticles,[40,41] and quantum dot (QDs)[42,43] have also been attempted to address the cytotoxicity and biocompability aspects of nanoparticles. The concentration of SERS NPs used in our work was several fold lower (5 nM *vs* 25 μM) than the past studies. Nevertheless, the toxicity of SERS NPs were evaluated at two different concentrations by following the morphological development of the NPs injected embryos compared with the uninjected probes as shown in Figure 3 (high concentration) and Supporting Information Figure S3 (low concentration). Images of the development of SERS NPs injected embryos and uninjected embryos (used as control) were obtained using a stereomicroscope (Olympus SZX16 with SDF PLAPO 0.8× lens) fitted with a digital camera (Olympus DP71) over a course of 7 days post fertilization. At the 18-somite stage, morphological development of somites (body musculature) along the anterior−posterior body axis was observed. Consistent with our *in situ* hybridization results, somites in NP injected embryos develop normally compared to the wild-type (Figure 4 panels E and F). After 4 days of development (after hatching), a larval fish was capable of responding to touch, suggesting that the central nervous system appears intact. After 7 days of development, a normal looking larval fish with a good balance and ability to feed on live paramecia was observed. Most of the organs such as those in the cardiovascular system and other organs such as the eye movement and muscles were found to function normally compared to the uninjected controls. As shown in the Supporting Information (video animation of blood flow),

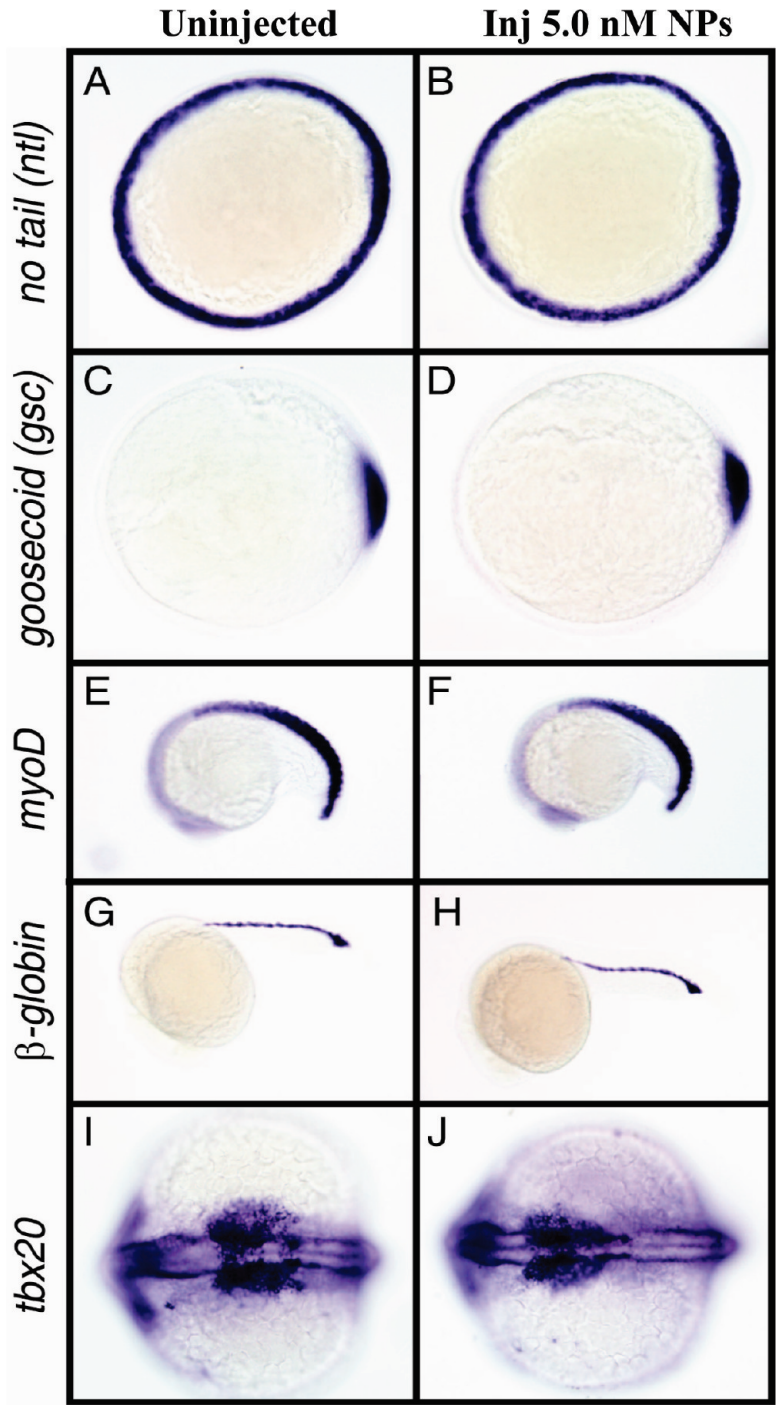

Figure 4. Expression of genes in SERS NP-injected and uninjected control embryo during development. (A−D) Animal views with dorsal to the right. (A,B) expression of no tail in the mesoderm of uninjected (A) and SERS NPs injected (B) embryos at the stage of 40% epiboly. (C, D) Expression of goosecoid (gsc) in the dorsal domain of uninjected (C) and SERS NPs injected (D) embryos at the stage of 40% epibobly. (E−H) Lateral views with anterior to the left. (E, F) expression of myoD in the developing somites along the anterior−posterior body axis of uninjected (E) and SERS NP injected (F) embryos at the 18-somite stage. (G, H) Expression of b-globin in the vasculature of uninjected (G) and SERS NPs injected embryos at 24 hpf. (I, J) Dorsal views with anterior to the left. Expression of tbx20 in developing cardiac regions of uninjected (I) and SERS NP injected (J) embryos.

the blood circulation and mechanical function of the cardiac chambers of the wild-type embryo and SERS NPs injected embryos were not affected clearly demonstrating that the physiological function of embryos were not affected.

Gene Expression Profiles of Embryos Injected with SERS NPs at Various Stages of Development. During development, cell-fate is determined by the expression of genes, which is activated spatially and temporally by combinatorial signaling pathways. Injection of SERS NPs may lead to

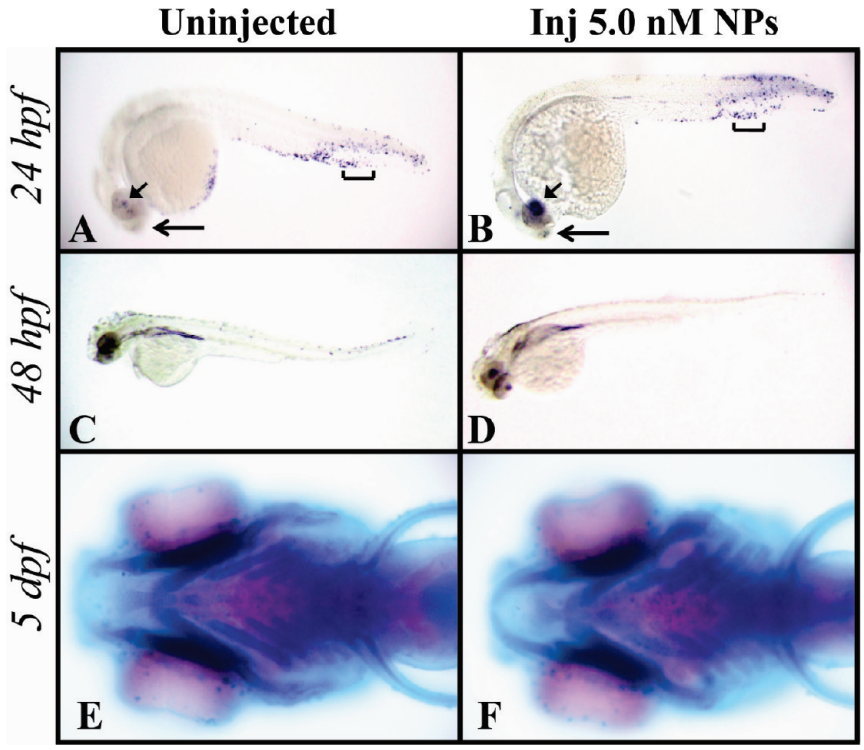

Figure 5. Analysis of uninjected and SERS probe injected embryos using *in situ* TUNEL and dual color skeletal staining assays. (A−D) Lateral views with anterior to the left. (A, B) *In situ* TUNEL assays of (A) uninjected and (B) injected embryos at 24 hpf. Arrowheads indicate the eye region, black arrows indicate the forebrain and black bracket marks the tail region. (C, D) *In situ* TUNEL assays of (C) uninjected and (D) injected embryos at 48 hpf. (E, F) Lateral views with anterior to the left of (E) uninjected, and (F) injected embryos at 5 day postfertilization (dpf). Close-up ventral views with anterior to the left of panels E and F showing the normal development of the pharyngeal skeleton.

disruption of normal gene expression that is too subtle to detect by morphological observation, and it is therefore important to examine the patterns of gene expression in embryos containing SERS NPs at various stages of development. During embryogenesis, no tail (ntl), a member of the T-box transcription factor family and an early marker for the induction of mesoderm that gives rise to the posterior body structures (Figure 4A) was monitored. We found that the expression of ntl is properly induced in both SERS NP injected and uninjected embryos at the stage of 40% epiboly (Figure 4A,B). Since the dorsal and ventral regions could not be distinguished by the expression of ntl at this stage, the expression of goosecoid (gsc), a member of the homeobox transcription factor family, which is a dorsal specific marker was examined. We found that, gsc appeared normal in SERS NPs injected embryos compared to the control (Figure 4C,D). These findings suggest that the specification and patterning of the distinct dorsal-ventral cell fates of the mesodermal progenitor cells occurred normally in embryos with SERS NPs. After gastrulation, the mesoderm is known to give rise to structures such as muscles, blood, and heart. Specific molecular markers were used to examine the formation of these mesodermal structures at different stages of development. At the 18-somite stage, the expression of myoD, muscle specific marker, in developing somites along the anterior−posterior body axis was examined and the myoD expression was found to be normal in developing somites which eventually could give rise to the musculature of the posterior body (Figure 4E,F). The expression of β-globin, a blood specific marker and tbx20 in the cardiac structure was found to be unaltered at 24 hpf (Figure 4G−J). Overall, gene expression profile shows that the SERS NPs do not have any detrimental effects in embryo development. Collectively, our data suggests that SERS NPs even at the highest concentration (5 nM) used in this study shows excellent biocompatibility and no cytotoxicity.

Whole-Mount *in Situ* TUNEL and Dual Color Skeletal Staining Assays. To further demonstrate the apparent lack of toxicity of SERS probes in the development of zebrafish embryos, *in situ* TUNEL assays were performed to detect apoptotic cells. At 24 hpf, a slight increase in apoptotic cell death was observed in the tail region of injected embryos (Figure 5B, black bracket), compared to the control embryos (Figure 5A, black bracket). Interestingly, injected embryos with low concentration of SERS NPs showed significantly lower levels of apoptotic cell death compared to control embryos (Supporting Information Figure S5C, black bracket). These results are consistent with our previous findings of the observed normal development of SERS probe injected embryos for up to 7 days (Figure 3). Dual color staining to examine the development of cartilage and bone of uninjected and SERS probe injected zebrafish embryos at 5

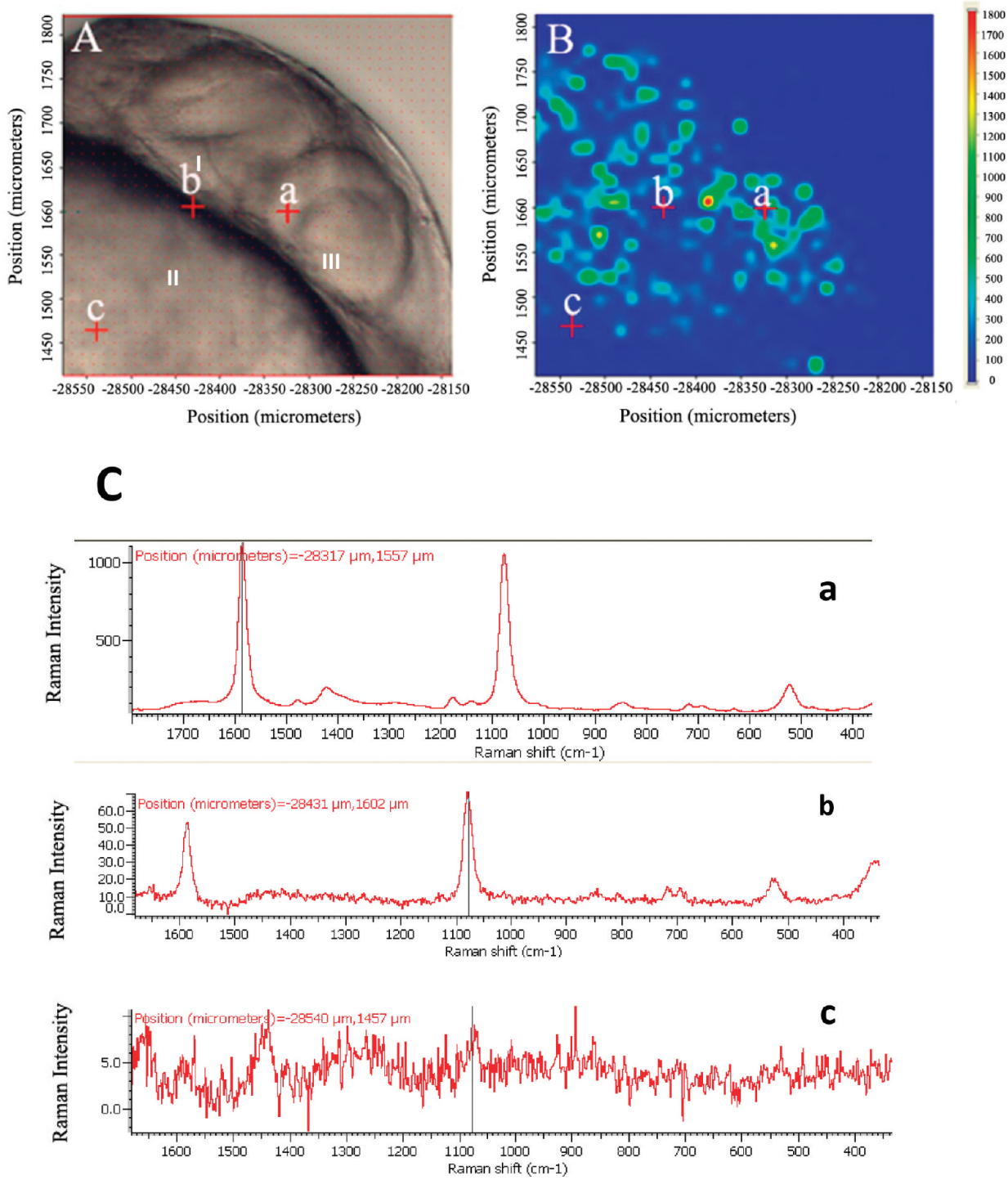

Figure 6. Raman mapping of the dorsal region of zebrafish embryo (14−16 hpf) injected with SERS NPs. (A) Optical image of the dorsal region of the zebrafish embryo and the markers highlight representative areas: (I) forebrain, (II) hatching gland, (III) eye. (B) SERS intensity map of the C−C vibration band from SERS NPs at 1078 cm^{-1}. (C) SERS spectra collected from three different points of the head as shown in panels A and B.

day postfertilization showed no obvious difference in the development of the pharyngeal skeleton between SERS probe injected and uninjected control embryos (Figure 5E,F). These findings suggest that the SERS probes used in this study at the indicated concentrations do not have any detectable toxic effects on embryo development.

Distribution of NPs in Embryos at Different Stages of Development by SERS Imaging. In recent years, studies relating to the distribution of nanoparticles in cells and tissues have attracted increased attention because of the potential that NPs in cells could be used for diagnostic and therapeutic purposes. Past research has demonstrated that TEM and fluorescence imaging are the most

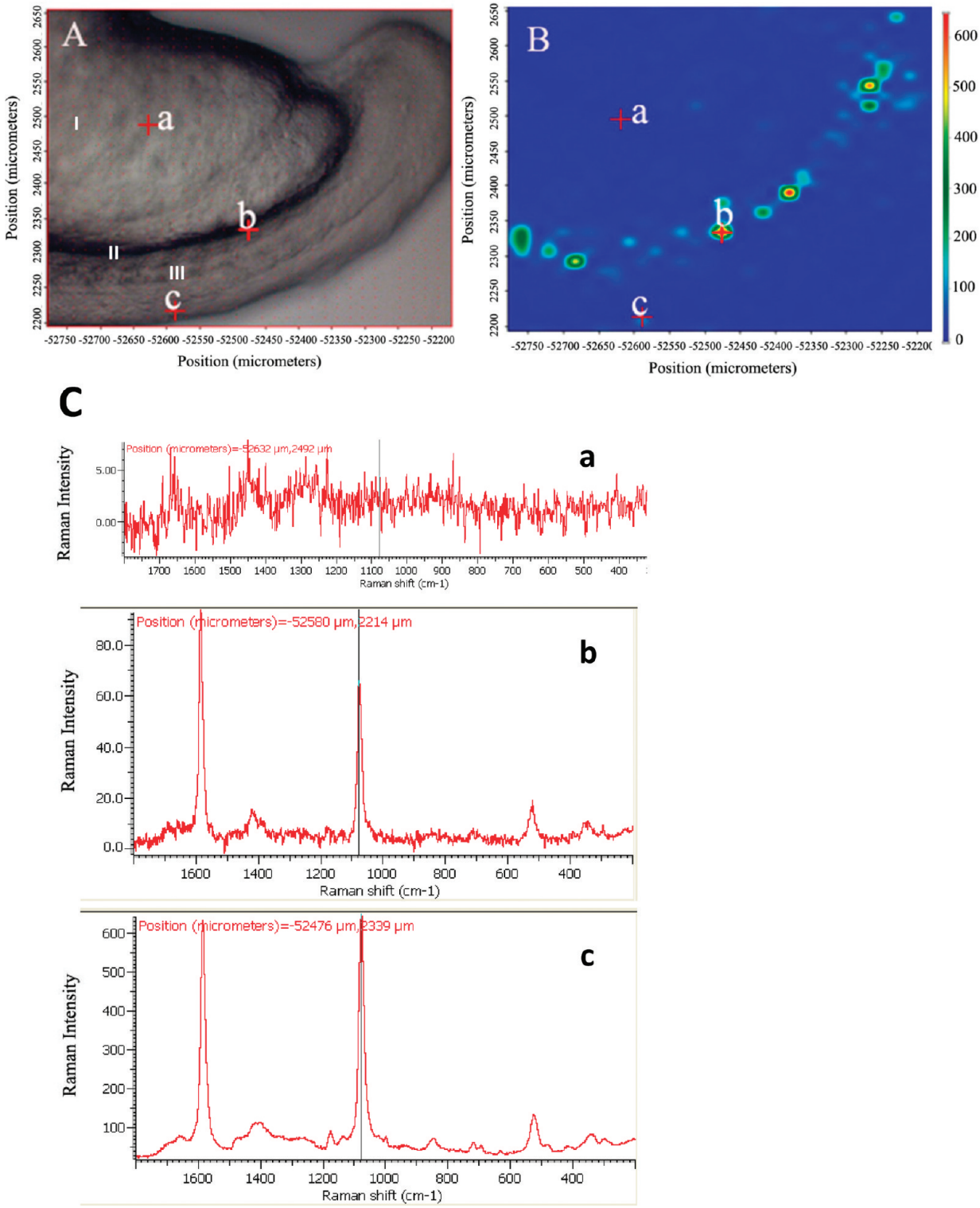

Figure 7. Raman mapping of the body musculature of the zebrafish embryo (14−16 hfp) injected with SERS NPs. (A) The optical image of the body musculature of the zebrafish embryo and the markers highlight representative areas: (I) yolk, (II) vechal vein, (III) somite. (B) SERS intensity maps of C−C vibration band from SERS NPs at 1078 cm^{-1}. (C) SERS spectra collected from three different points of the embryo shown in panels A and B.

widely employed techniques for direct examination of NPs in single cells.[44,45] Imaging by TEM is effective for static observation but is a destructive technique. Although fluorescence has its advantages in *in vivo* imaging of cells or animal models, photobleaching, background cellular autofluorescence, and lack of single molecule sensitivity are challenges to overcome. Raman mapping based on SERS can be used for multiplex noninvasive *in vivo* monitoring of targets at single particle sensitivity. Here, Raman mapping was used to

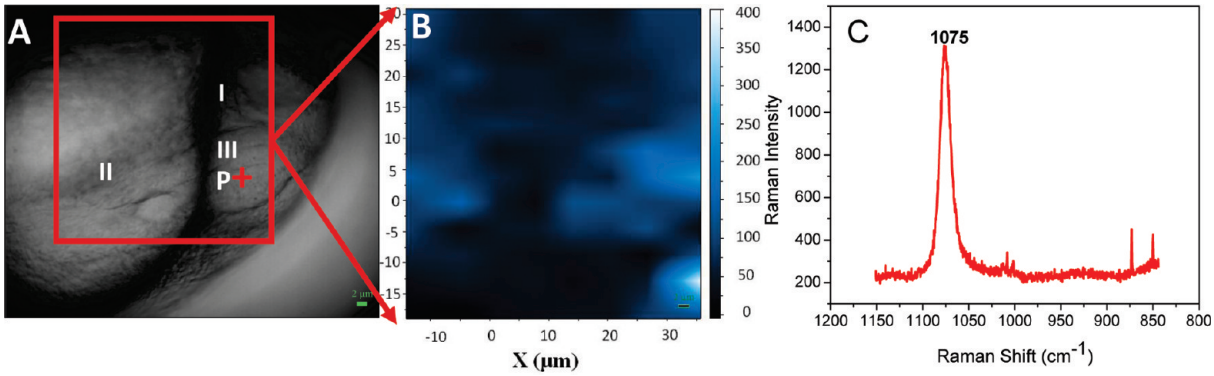

Figure 8. Raman mapping of the dorsal region of zebrafish embryo at the developmental stage of 20−22 hpf. (A) The optical image of the dorsal region of zebrafish embryo and the markers highlight representative areas: (I) forebrain, (II) ventral brain, (III) eye. (B) SERS intensity maps of C−C vibration band from SERS NPs at 1078 cm^{-1}. (C) Typical SERS spectrum collected from the point marked by P as shown in A.

track the distribution of SERS NPs (5 nM) in zebrafish embryos microinjected into the one-cell stage. The biodistribution of SERS NPs was first documented in two separate regions of the embryo at 14−16 hpf as indicated in Figures 6 and 7. Figure 6A gives the optical image of the anterior view of the embryo at the 14−16 hpf and 6B gives the Raman map of the entire area of A. Figure 6C gives the SERS spectra obtained from the point indicated in Figure 6 panels A and B. From the images, it is obvious that the SERS NPs were distributed in the anterior region that included the forebrain, eyes, and hatching gland. The distribution of SERS NPs in the body musculature of the same zebrafish embryo of Figure 6 is illustrated in Figure 7. Figure 7A,B provides the optical and SERS image of the body musculature of the zebrafish embryo, among which, spectra a, b, and c are obtained from the yolk, the ventral vein, and somite regions of the body musculature, respectively. Our

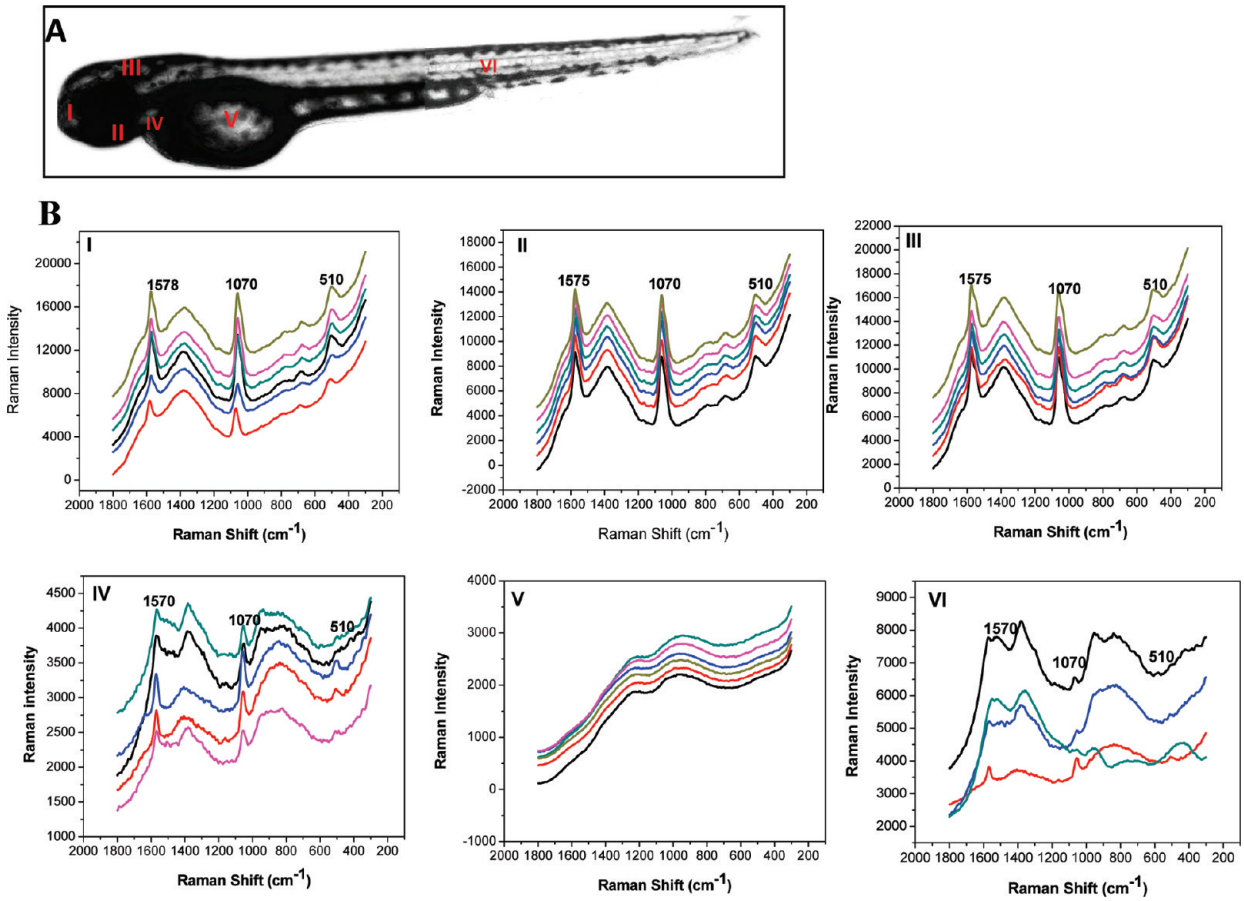

Figure 9. Characterization of SERS NPs embedded inside a fully developed (48 hpf) zebrafish using SERS measurement. (A) Optical image of a normally developed zebrafish. The red markers highlight representative areas: (I) forebrain, (II) pharyngeal skeleton, (III) hindbrain, (IV) heart, (V) yolk, and (VI) somite. (B) SERS spectra obtained from those tissue sections outlined in panel A.

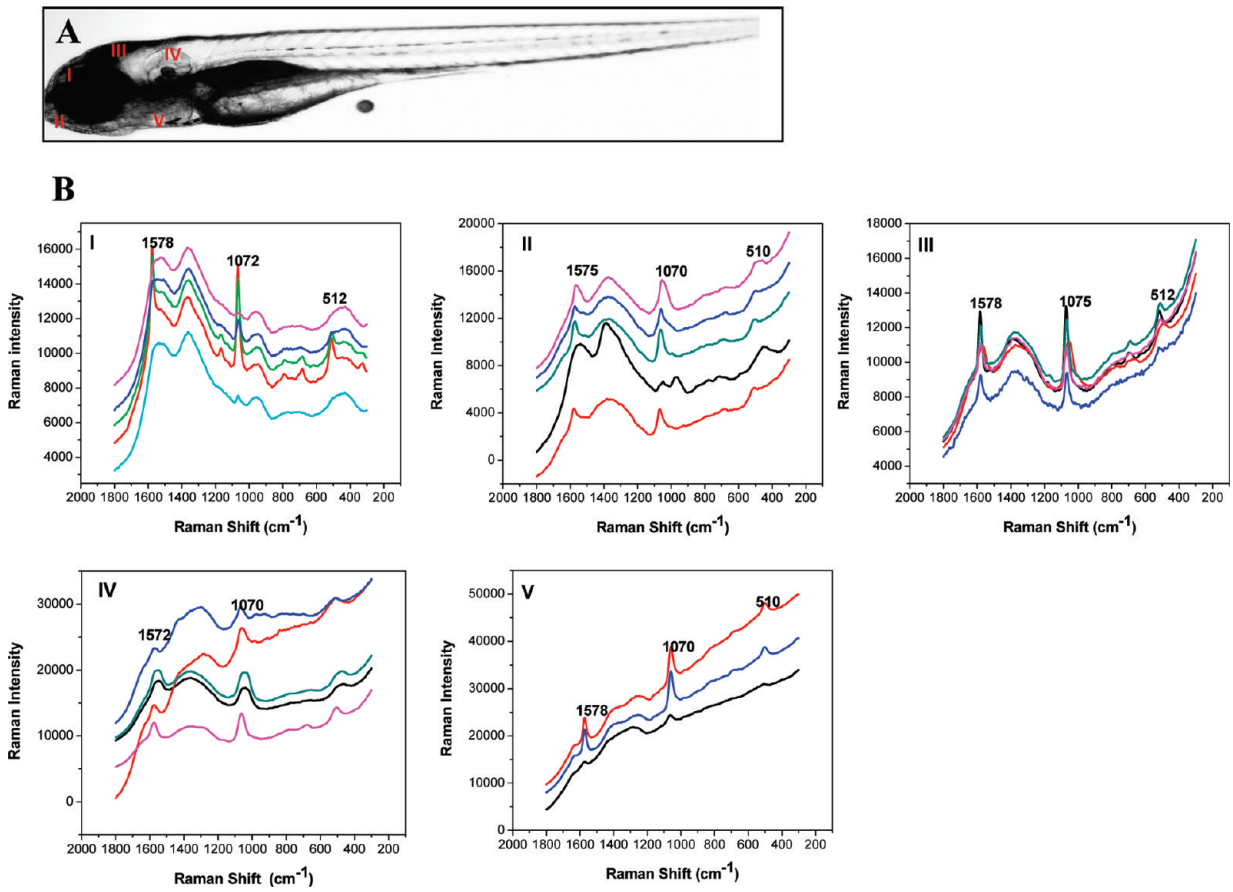

Figure 10. Characterization of SERS NPs embedded inside a fully developed (96 hpf) zebrafish using SERS measurement. (A) Optical image of a normally developed zebrafish. The red markers highlight representative areas: (I) forebrain, (II) mouth, (III) hindbrain, (IV) otic vesicle, and (V) heart. (B) SERS spectra obtained from those tissue sections outlined in panel A.

results indicate that a SERS signal could be detected in different tissues in developing zebrafish embryos, but not in the yolk tube. Moreover, the injected embryos developed indistinguishably from uninjected embryos (as shown in Figure 3) to give a unique SERS signal throughout the embryo. The observed distribution of SERS NPs in the various tissues of the embryo indicates that the injected NPs were able to spread to different blastomeres during the cleavage stage of development and ultimately into different organs and tissue progenitor cells as these regions develop in the entire zebrafish organism.[43] It has been reported by Kneipp *et al.* that the state of AuNPs in the cell varies with time, and after 24 h AuNPs aggregated to form small AuNPs clusters in the cytoplasm.[46] In our experiments, two processes were expected to cause the SERS NPs to distribute randomly throughout the tissues or organs in the zebrafish embryo even though the SERS NPs were microinjected at the one-cell stage. The first is a process similar to that observed by Kneipp *et al.*,[46] implying that NPs will aggregate to form small clusters with time in the cytoplasm. The other is a dynamic process where some SERS NPs localize in the cells as they divide. To confirm our assumption, SERS spectra obtained from embryos incubated or microinjected with NPs under ideal conditions were compared. As shown in Supporting Information Figure S5, the SERS signal obtained from embryos with probes uptaken by incubation was much stronger than the signal from embryos with microinjected probes. As reported by Lee *et al.*,[26] during incubation, the nanoparticles initially trapped will serve as the nucleation site to initiate the formation of aggregates with the incoming nanoparticles to form larger particle aggregates; that gives rise to a strong SERS signal (Supporting Information Figure S5). This is also expected because during the process of incubation (~20 h) the embryos uptake nanoparticles which redistribute as the cells divide, at the same time providing ample opportunity for the internalization of additional particles that are uptaken by embryos. Therefore, incubation may not be a viable method for intracellular tracking because it is not possible to localize the probes to a specific region or track the trajectory from the inception. Microinjection will minimize or eliminate the aggregation of nanoparticles and facilitate its distribution into the different regions.

To observe the time-dependent distribution of SERS NPs in the embryo, Raman mapping was performed on zebrafish embryos at the 20−22 hpf (Figure 8), where an optical image, Raman map of the selected section, and a typical SERS spectra obtained from the embryos were provided. From the image, the random

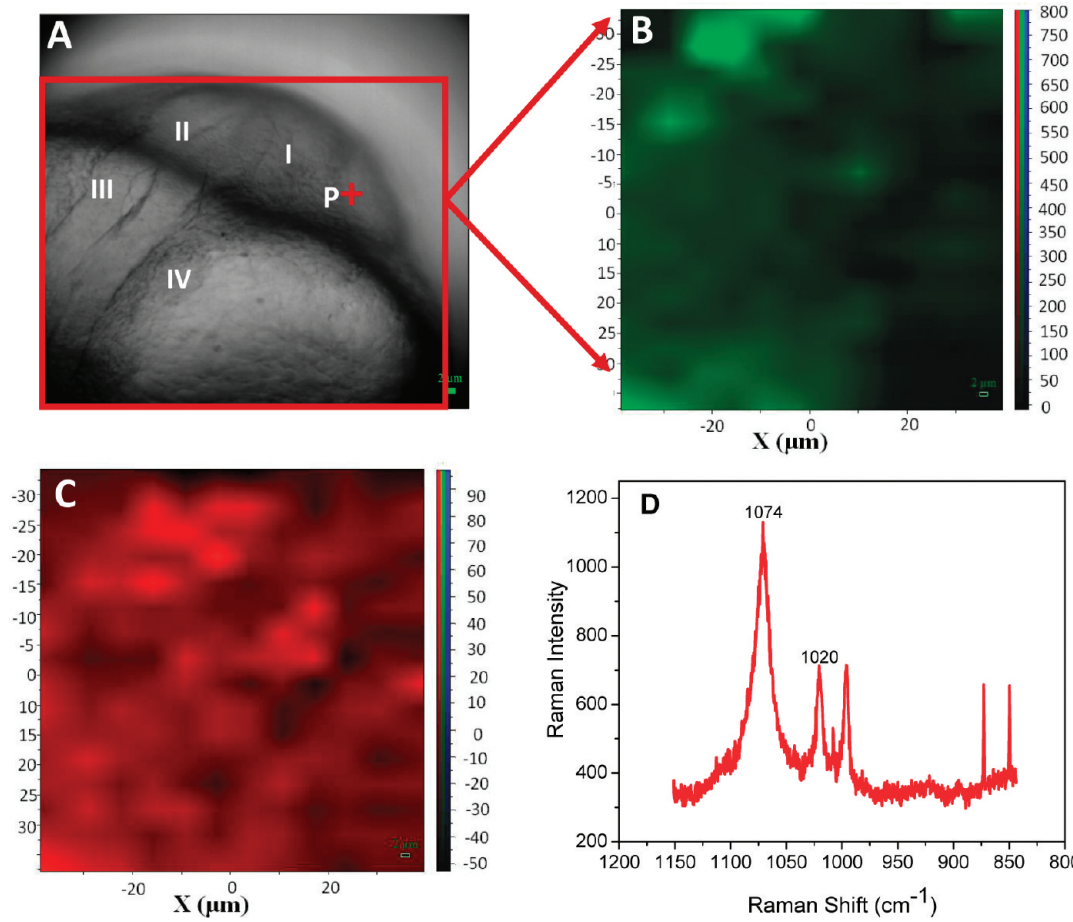

Figure 11. Multiplex Raman mapping of two SERS NPs in the dorsal region of zebrafish embryo. (A) The optical image of the dorsal region of zebrafish embryo (18−20 hpf) and the markers highlight representative areas: (I) forebrain, (II) midbrain, (III) hindbrain, (IV) otic vesicle. (B) SERS intensity map of C−C vibration band from SERS NPs-1 at 1078 cm^{-1}, and (C) SERS intensity map of ring breathing vibration band from SERS NPs-2 at 1020 cm^{-1}. (D) Typical SERS spectrum collected from the point marked by P as shown in A.

distribution of SERS NPs along the dosal region of the zebrafish embryo could be observed and no signal was observed from the yolk, consistent with the results obtained from the early embryos as shown in Figures 2, 6, and 7. Results indicate that Raman mapping can serve as an excellent platform to study the distribution of SERS NPs in different tissues and organs in developing embryo.

To more clearly ascertain the distribution and accumulation of NPs in different organs of zebrafish embryo, Raman measurements were obtained from different organs of the embryos at 48 hpf and 96 hpf as shown in Figure 9 and Figure 10, respectively. It can be seen that SERS NPs will distribute into multiple organs (brain, mouth, pharyngeal skeleton, otic vesicle, and tail) of normally developing zebrafish from the initial one-cell stage, conclusively demonstrating that SERS NPs can compartmentalize into different cells as the cells divide. Furthermore, we note that as the cells divide, the number of SERS NPs in each cell decreases to produce a weaker signal with cell division as shown in the SERS spectra from the tail of developing embryos.

Multiplex Imaging of SERS NPs in the Live Embryos. Simultaneous detection of multiple molecules is attractive because different targets can be traced *in vivo*. Multiplex SERS imaging *in vivo* was demonstrated by coinjecting two different SERS NPs (mercaptobenzoic acid, MBA, and mercaptopyridine, MPY) in a 1:1 ratio at the one-cell stage. These probes are respectively termed as SERS NPs-1 and SERS NPs-2. The SERS spectra (Supporting Information Figure S6) show typical vibration bands of the two probes separately in the embryo and when co-injected. The spectrum obtained from embryos co-injected with the two probes represents the combination of Raman signals obtained from each of the two SERS NPs. Raman maps of the two SERS NPs were obtained to assess the distribution of the two coinjected probes in the embryo. The first study was carried out in the dosal region of embryos at the 18−20 hpf (Figure 11A, optical image). Figure 11D shows the vibration bands from a typical SERS spectra from embryos co-injected with the two probes. Raman maps were subsequently obtained corresponding to the 1020 cm^{-1} band of SERS NPs-2 (assigned to the ring breathing vibration of MPY[47,48]) and 1078 cm^{-1} band of SERS NPs-1 lines (assigned to the C−C vibration of MBA),

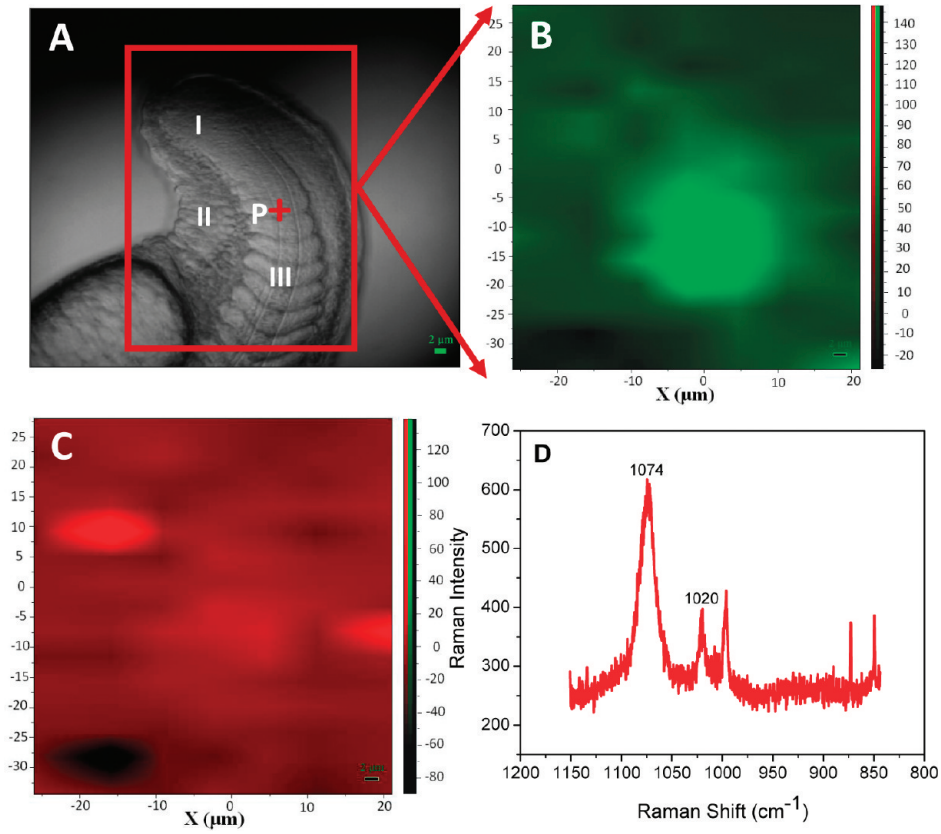

Figure 12. Raman mapping of two SERS NPs in the posterior region of zebrafish embryo: (A) optical image of the zebrafish embryo (18−20 hpf) and the markers highlight representative areas: (I) presomitic mesoderim, (II) blood island, (III) somite. (B) SERS intensity map of the C−C vibration band from SERS NPs-1 at 1078 cm^{-1} and (C) SERS intensity map of ring breathing vibration band from SERS NPs-2 at 1020 cm^{-1}. (D) Typical SERS spectrum collected from the point marked by P as shown in panel A.

respectively (indicated in Figure 10B,C), representing the location of the two probes in the same embryo. Further experiments into the posterior region of the embryos from the same 18 to 20 somite stage (Figure 12) show the distribution of the two SERS NPs after injection at the one-cell stage. The multiplex SERS image (Figure 12B,C) along the posterior region of the embryo indicates that the two NPs will experience the same process discussed above and tend to distribute throughout the whole embryo. However, if the SERS NPs were functionalized with specific cell surface markers targeting different cell types the development of specific organs and tissues during the development process can be monitored. Given the choice of nonfluorescent probes demonstrated in our earlier work,[49] 4−8 different cell types could be simultaneously monitored by SERS imaging.

SUMMARY

Understanding the biocompatibility and biodistribution of nanosensors in a living system is one of the key requirements of nanomedicine. We utilize zebrafish embryo as a platform to track the distribution and assess the biocompatibility of SERS NPs *via in vivo* and multiplex Raman chemical imaging. Our proof-of-concept study demonstrates that microinjected SERS NPs at the one-cell stage could distribute into different tissues and organs of zebrafish embryos during development. The normal morphology of SERS NP-injected zebrafish embryos was assessed by the expression of molecular markers to confirm the expression of genes at various stages suggesting that the embryos are normal and the probes are not toxic. By multiplex SERS imaging we confirm the detection and distribution of two nonfluorescent probes in zebrafish embryo microinjected at the one-cell stage. To conclude, SERS could be a powerful tool for monitoring multiple targets simultaneously during embryo development with single molecule sensitivity. Thus intricate physiological and pathological processes in embryo development could be monitored. Our study will set the stage for developing a comprehensive Raman imaging platform for multiplex *in vivo* detection and quantification of cell phenotypes in zebrafish models.

MATERIALS AND METHODS

Chemical Reagents. Hydrogen tetrachloroaurate (III) trihydrate ($HAuCl_4 \cdot 3H_2O$, 99%), sodium citrate dehydrate, 4-mercaptobenzoic acid (MBA), and 4-mercaptopyridine (MPY) were obtained from Sigma-Aldrich Chemical Co. and used without further purification. Water was purified with Milli-Q plus

system (Millipore Co.) and the resistivity was assessed to be $>18\ M\Omega \cdot cm$.

Preparation of SERS NPs. All glassware used in the following procedures was thoroughly cleaned in a bath of freshly prepared 3:1 HCl:HNO_3 (aqua regia), rinsed with Milli-Q water and oven-dried prior to use. AuNPs of different sizes were synthesized by aqueous reduction of $HAuCl_4$ with sodium citrate according to Frens's method.[50]

Two different Raman labels were used, SERS NPs-1 composed of AuNPs and MBA, and SERS NPs-2 composed of AuNPs with MPY. SERS NPs-1 was fabricated by functionalizing AuNPs labeled by MBA (AuNPs−MBA) with modification.[51] Approximately 150 μL of 1 mM MBA was added to 15 mL of the as-prepared AuNPs in a NaOH-treated glass vial with magnetic stirring to facilitate the reaction for 12 h. The contents were then centrifuged at 8000 rpm for the 25 nm AuNPs and at 6000 rpm for the 40 nm AuNPs at room temperature for 15 min twice to remove free MBA prior to use. The SERS NPs-2 comprising AuNPs and MPY was prepared using a similar process. After centrifugation, 1.5 mL of SERS NPs were redispersed in 120 and 30 μL water, respectively, to obtain two different concentrations (1.25 and 5 nM) of SERS NPs for embryo experiments.

TEM Instrument. The size and morphology of AuNPs were obtained from transmission electron microscopy (TEM), using a Philips CM-100 TEM (Philips, Eindhoven, Netherlands) operating at 100 kV.

UV−Visible Absorption Instrument. Absorption spectra of AuNPs and SERS NPs were measured with a Jasco V570 UV/visible/NIR spectrophotometer (Jasco, Inc., Easton, MD) in the wavelength range from 400 to 900 nm.

Raman Measurements. NIR-SERS spectral acquisition for zebrafish embryo was conducted using the SENTERRA confocal Raman system (Bruker Optics Inc., Billerica, MA) with a 20× air objective with a 785 nm excitation laser with a 50 μm pinhole for confocality. The laser power and accumulation time were 10 mW and 10 s, respectively.

Raman Mapping was carried out using the DXR Raman microscopy (Thermo Fisher Scientific Inc. Waltham, MA) with a computer-controlled *x,y* stage in a 12 μm step size for the tail of embryo and 14 μm step size for the head of the embryo at 780 nm excitation. The excitation intensity and accumulation time was 10 mW and 10 s, respectively.

Before each Raman measurement, zebrafish embryos were anesthetized with tricaine in accordance with the approved animal protocol of Purdue University.

Embryos and Microinjection. Zebrafish embryos (*Danio rerio*) were obtained by natural spawning of the adult AB strain of zebrafish. Embryos were raised and maintained at 28.5 °C in system water and staged as described.[52] Embryos were first collected at the one-cell stage, transferred into an injection tray containing system water, and the cell of the embryo was oriented to directly face the injection needle. SERS NPs were then injected directly inside the cell of embryo at the one-cell stage. Each embryo was injected with approximately 1 nL volume of SERS probe using a Picospritzer III (Parker Hannifin). Scheme 1 shows the schematic of this microinjection step. Embryos were then collected at appropriate stages for visual observation using stereomicroscope, Raman experiments, and *in situ* hybridization tests. The amount of SERS NPs corresponding to an injected volume of 5×10^{-18} mole can approximately be estimated to be 3×10^6 particles.

Whole-Mount *in Situ* Hybridization and TUNEL and Dual Color Skeletal Staining Assays. Embryos were collected at the appropriate stages and fixed in 4% paraformaldehyde, pH 7.0, in phosphate-buffered saline (PBS), overnight at 4 °C. Fixed embryos were dechorionated, washed three times with PBS, and stored in methanol at −20 °C. Whole-mount *in situ* hybridization was performed using digoxigenin-labeled antisense RNA probes and visualized using antidigoxigenin Fab fragment conjugated with alkaline phosphatase (Roche Corp.) as previously described.[6] Riboprobes were made from DNA templates, linearized and transcribed with either SP6 or T7 RNA polymerases. Embryos were processed and hybridized as previously described.[6] Whole-mount *in situ* TUNEL (terminal deoxynucleotide transferase-mediated dUTP nick-end labeling) was performed using the AP (alkaline phosphatase). *In situ* Cell Death Detection Kit (Roche Corp.) was performed as previously described.[53] Whole-mount dual color staining was carried out as described.[54]

Acknowledgment. Partial funding for this work was provided by the Showalter trust grant from Purdue University and the NSF IDBR grant to J.I. (co-PI) and Purdue startup grant to D.S.

Supporting Information Available: Figure S1 gives the SERS spectra of Raman reporters functionalized with SERS probes of two different diameters in bulk solution and in live zebrafish embryo with control; Figure S2 compares the SERS spectra of Raman reporters functionalized NPs in bulk solution and in live embryos at two different concentrations; Figure S3 provides microscopic images of wild-type embryo and embryos injected with 1.25 nM concentration of SERS NPs; Figure S4 shows the analysis of uninjected and SERS probe injected embryos using *in situ* TUNEL and dual color skeletal staining assays. Figure S5 shows the SERS spectra from zebrafish embryo incubated with SERS NPs. Figure S6 gives the spectra from embryos injected separately and co-injected with two different SERS NPs, respectively. Scheme S1 shows the fate map of the deep cell layer at 6−8 hpf. Two real-time videos, movies 1 and 2, illustrate the blood flow in the heart and vasculature of the wild-type and injected zebrafish embryo 7 days old, respectively. This material is available free of charge via the Internet at http://pubs.acs.org.

REFERENCES AND NOTES

1. Hardt, S.; Bakkers, J.; Inbal, A.; Carvalho, L.; Solnica-Krezel, L.; Heisenberg, C.-P.; Hammerschmidt, M. The Bmp Gradient of the Zebrafish Gastrula Guides Migrating Lateral Cells by Regulating Cell−Cell Adhesion. *Curr. Biol.* **2007**, *17*, 475–487.
2. Tucker, J. A.; Mintzer, K. A.; Mullins, M. C. The BMP Signaling Gradient Patterns Dorsoventral Tissues in a Temporally Progressive Manner along the Anteroposterior Axis. *Developmental Cell* **2008**, *14*, 108–119.
3. Gritsman, K.; Zhang, J.; Cheng, S.; Heckscher, E.; Talbot, W. S.; Schier, A. F. The EGF−CFC protein one-eyed pinhead is essential for nodal signaling. *Cell* **1999**, *97*, 121–132.
4. Schier, A. F.; Talbot, W. S. Molecular genetics of axis formation in zebrafish. *Annu. Rev. Genet.* **2005**, *39*, 561–613 (Review).
5. Szeto, D. P.; Kimelman, D. The regulation of mesodermal progenitor cell commitment to somitogenesis subdivides the zebrafish body musculature into distinct domains. *Genes Dev.* **2006**, *20*, 1923–1932.
6. Szeto, D. P.; Kimelman, D. Combinatorial gene regulation by Bmp and Wnt in zebrafish posterior mesoderm formation. *Development* **2004**, *131*, 3751–3760 (Erratum: *Development,* **2004**, *131*, 4117).
7. Jun, Y. W.; Huh, Y. M.; Choi, J. S.; Lee, J. H.; Song, H. T.; Kim, S. J.; Yoon, S.; Kim, K. S.; Shin, J. S.; Suh, J.-S.; *et al.* Nanoscale Size Effect of Magnetic Nanocrystals and Their Utilization for Cancer Diagnosis *via* Magnetic Resonance Imaging. *J. Am. Chem. Soc.* **2005**, *127*, 5732–5733.
8. Gorantla, S.; Dou, H. Y.; Boska, M.; Destache, C. J.; Nelson, J.; Poluektova, L.; Rabinow, B. E.; Gendelman, H. E.; Mosley, R. L. Quantitative Magnetic Resonance and SPECT Imaging for Macrophage Tissue Migration and Nanoformulated Drug Delivery. *J. Leukocyte. Biol.* **2006**, *80*, 1165–1174.
9. Ma, L. L; Feldman, M. D; Tam, J. M; Paranjape, A. S; Cheruku, K. K; Larson, Ti. A; Tam, J. O; Ingram, D. R; Paramita, V.; Villard, J. W; *et al.* Small Multifunctional Nanoclusters (Nanoroses) for Targeted Cellular Imaging and Therapy. *ACS Nano* **2009**, *3*, 2686–96.
10. Mu, C. J.; LaVan, D. A.; Langer, R. S.; Zetter, B. R. Self-Assembled Gold Nanoparticle Molecular Probes for Detecting Proteolytic Activity *in Vivo*. *ACS Nano* **2010**, *4*, 1511–1520.
11. Hu, Q.; Tay, L.; Noestheden, M.; Pezacki, J. P. Mammalian Cell Surface Imaging with Nitrile-Functionalized Nanoprobes: Biophysical Characterization of Aggregation

and Polarization Anisotropy in SERS Imaging. *J. Am. Chem. Soc.* **2007**, *129*, 14–15.
12. Driskell, J. D.; Kwarta, K. M.; Lipert, R. J.; PorterJohn, M. D.; Neill, D.; Ridpath, J. F. Low-Level Detection of Viral Pathogens by a Surface-Enhanced Raman Scattering Based Immunoassay. *Anal. Chem.* **2005**, *77*, 6147–6154.
13. Sun, L.; Sung, K. B.; Dentinger, C.; Lutz, B.; Nguyen, L.; Zhang, J.; Qin, H.; Yamakawa, M.; Cao, M.; Lu, Y.; *et al.* Composite Organic−Inorganic Nanoparticles as Raman Labels for Tissue Analysis. *Nano Lett.* **2007**, *7*, 351–356.
14. Fleishchman, M.; Hendra, P. J.; McQuillan, A. J. Raman Spectra of Pyridine Adsorbed at a Silver Electrode. *Chem. Phys. Lett.* **1974**, *26*, 163–166.
15. Nie, S. M.; Emery, S. R. Probing Single Molecules and Single Nanoparticles by Surface-Enhanced Raman Scattering. *Science.* **1997**, *275*, 1102–1106.
16. Kneipp, K.; Wang, Y.; Kneipp, H.; Perelman, L. T.; Itzkan, I.; Dasari, R.; Feld, M. S. Single Molecule Detection Using Surface-Enhanced Raman Scattering (SERS). *Phys. Rev. Lett.* **1997**, *78*, 1667.
17. Ryder, A. G. Surface-Enhanced Raman Scattering for Narcotic Detection and Applications to Chemical Biology. *Curr Opin Chem Biol.* **2005**, *9*, 489–493.
18. Kneipp, J.; Kneipp, H.; Rice, W. L.; Kneipp, K. Optical Probes for Biological Applications Based on Surface-Enhanced Raman Scattering from Indocyanine Green on Gold Nanoparticles. *Anal. Chem.* **2005**, *77*, 2381–2385.
19. Tang, H. W.; Yang, X. B.; Kirkham, J.; Smith, D. A. Probing Intrinsic and Extrinsic Components in Single Osteosarcoma Cells by Near-Infrared Surface-Enhanced Raman Scattering. *Anal. Chem.* **2007**, *79*, 3646–3653.
20. Wang, Y.; Li, D.; Li, P.; Wang, W.; Ren, W.; Dong, S.; Wang, E. Surface Enhanced Raman Scattering of Brilliant Green on Ag Nanoparticles and Applications in Living Cells as Optical Probes. *J. Phys. Chem. C* **2007**, *111*, 16833–16839.
21. Keren, S.; Zavaleta, C.; Cheng, Z.; Zerda, A; Gheysens, O; Gambhir, S. S. Noninvasive Molecular Imaging of Small Living Subjects Using Raman Spectroscopy. *Proc. Natl. Acad. Sci. U.S.A.* **2008**, *15*, 5844–5849.
22. Zavaleta, C.; de la Zerda, A.; Liu, Z.; Keren, S.; Cheng, Z.; Schipper, M.; Chen, X.; Dai, H.; Gambhir, S. S. Noninvasive Raman Spectroscopy in Living Mice for Evaluation of Tumor Targeting with Carbon Nanotubes. *Nano Lett.* **2008**, *8*, 2800–2805.
23. Qian, X.; Peng, X. H.; Ansari, D. O.; Goen, Q. Y.; Chen, G. Z.; Shin, D. M.; Yang, L.; Young, A. N.; Wang, M. D.; Nie, S. M. *In Vivo* Tumor Targeting and Spectroscopic Detection with Surface-Enhanced Raman Nanoparticle Tags. *Nat. Biotechnol.* **2008**, *26*, 83–90.
24. Souza, G. R.; Levin, C. S.; Hajitou, A.; Pasqualini, R.; Arap, W.; Miller, J. H. *In Vivo* Detection of Gold-Imidazole Self-Assembly Complexes: NIR-SERS Signal Reporters. *Anal. Chem.* **2006**, *78*, 6232–6237.
25. Asharani, P. V.; Wu, Y. L.; Gong, Z.; Valiyaveettil, S. Toxicity of Silver Nanoparticles in Zebrafish Models. *Nanotechnology* **2008**, *19*, 1–8.
26. Lee, K. J.; Nallathamby, P. D.; Browning, L. M.; Osgood, C. J.; Xu, X.-H. N. *In Vivo* Imaging of Transport and Biocompatibility of Single Silver Nanoparticles in Early Development of Zebrafish Embryos. *ACS Nano* **2007**, *1*, 133–143.
27. Nallathamby, P. D.; Lee, K. J.; Xu, X.H. N. Design of Stable and Uniform Single Nanoparticle Photonics for *in Vivo* Dynamics Imaging of Nanoenvironments of Zebrafish Embryonic Fluids. *ACS Nano* **2008**, *2*, 1371–1380.
28. Zavaleta, C. L.; Smith, B. R.; Walton, I.; Doering, W.; Davis, G.; Shojaei, B.; Natan, M. J.; Gambhir, S. S. Multiplexed Imaging of Surface-Enhanced Raman Scattering Nanotags in Living Mice Using Noninvasive Raman Spectroscopy. *Proc. Natl. Acad. Sci. U.S.A.* **2009**, *106*, 13511–13516.
29. Xu, S.; Ji, X.; Xu, W.; Li, X.; Wang, L.; Yang, B.; Zhao, B.; Ozaki, Y. Immunoassay Using Probe-Labelling Immunogold Nanoparticles with Silver Staining Enhancement via Surface-Enhanced Raman Scattering. *Analyst.* **2004**, *129*, 63–68.
30. Orendorff, C. J.; Tapan, A. G.; Sau, K.; Murphy, C. J. Surface-Enhanced Raman Spectroscopy of Self-Assembled Monolayers: Sandwich Architecture and Nanoparticle Shape Dependence. *Anal. Chem.* **2005**, *77*, 3261–3266.
31. Kimmel, C. B.; Ballard, W. W.; Kimmel, S. R.; Ullmann, B.; Schilling, T. F. Stages of Embryonic Development of the Zebrafish. *Dev. Dyn.* **1995**, *203*, 253–310.
32. Lewinski, N.; Colvin, V.; Drezek, R. Cytotoxicity of Nanoparticles. *Small* **2008**, *4*, 26–49.
33. Goodman, C. M.; McCusker, C. D.; Yilmaz, T.; Rotello, V. M. Toxicity of Gold Nanoparticles Functionalized with Cationic and Anionic Side Chains. *Bioconjugate Chem.* **2004**, *15*, 897–900.
34. Tkachenko, A.; Xie, H.; Coleman, D.; Glomm, W.; Ryan, J.; Anderson, M. ; Franzen, S.; Feldheim, D. Multifunctional Gold Nanoparticle−Peptide Complexes for Nuclear Targeting. *J. Am. Chem. Soc.* **2003**, *125*, 4700–4701.
35. Tkachenko, A.; Xie, H.; Liu, Y.; Coleman, D.; Ryan, J.; Glomm, W.; Shipton, M.; Franzen, S.; Feldheim, D. Cellular Trajectories of Peptide-Modified Gold Particle Complexes: Comparison of Nuclear Localization Signals and Peptide Transduction Domains. *Bioconjugate Chem.* **2004**, *15*, 482–490.
36. Thomas, M.; Klibanov, A. Conjugation to Gold Nanoparticles Enhances Polyethylenimine'S Transfer of Plasmid DNA into Mammalian Cells. *Proc. Natl. Acad. Sci. U.S.A.* **2003**, *100*, 9138–9143.
37. Connor, E.; Mwamuka, J.; Gole, A.; Murphy, C.; Wyatt, M. Gold Nanoparticles Are Taken Up by Human Cells but Do Not Cause Acute Cytotoxicity. *Small* **2005**, *1*, 325–327.
38. Bar-Ilan, O.; Albrecht, R. M.; Fako, V. E.; Furgeson, D. Y. Toxicity Assessments of Multisized Gold and Silver Nanoparticles in Zebrafish Embryos. *Small* **2009**, *5*, 1897–1910.
39. Ispas, C.; Andreescu, D.; Patel, A.; Goia, D. V.; Andreescu, S.; Wallace, K. N. Toxicity and Developmental Defects of Different Sizes and Shape Nickel Nanoparticles in Zebrafish. *Environ. Sci. Technol.* **2009**, *43*, 6349–6356.
40. Van Hoecke, K.; Quik, J. T.; Mankiewicz-Boczek, J.; De Schamphelaere, K. A.; Elsaesser, A.; van der Meeren, P.; Barnes, C.; McKerr, G.; Howard, C. V.; van de Meent, D.; *et al.* Fate and Effects of CeO_2 Nanoparticles in Aquatic Ecotoxicity Tests. *Environ. Sci. Technol.* **2009**, *43*, 4537–4546.
41. Zhu, X.; Zhu, L.; Duan, Z.; Qi, R.; Li, Y.; Lang, Y. Comparative Toxicity of Several Metal Oxide Nanoparticle Aqueous Suspensions to Zebrafish (*Danio rerio*) Early Developmental Stage. *J. Environ. Sci. Health, A* **2008**, *43*, 278–284.
42. King-Heiden, T. C.; Wiecinski, P. N.; Mangham, A. N.; Metz, K. M.; Nesbit, D.; Pedersen, J. A.; Hamers, R. J.; Heideman, W.; Peterson, R. E. Quantum Dot Nanotoxicity Assessment Using the Zebrafish Embryo. *Environ. Sci. Technol.* **2009**, *43*, 1605–1611.
43. Rieger, S.; Kulkarni, R. P.; Darcy, D.; Fraser, S. E.; Köster, R. W. Quantum Dots Are Powerful Multipurpose Vital Labeling Agents in Zebrafish Embryos. *Dev. Dyn.* **2005**, *234*, 670–681.
44. Nativo, P.; Prior, L.; Brust, M. Uptake and Intracellular Fate of Surface-Modified Gold Nanoparticles. *ACS Nano* **2008**, *2*, 1639–1644.
45. Jin, H.; Heller, D. A.; Sharma, R.; Strano, M. S. Size-Dependent Cellular Uptake and Expulsion of Single-Walled Carbon Nanotubes: Single Particle Tracking and a Generic Uptake Model for Nanoparticles. *ACS Nano* **2009**, *3*, 149–158.
46. Kneipp, J.; Kneipp, H.; McLaughlin, M.; Brown, D.; Kneipp, K. *In Vivo* Molecular Probing of Cellular Compartments with Gold Nanoparticles and Nanoaggregates. *Nano Lett.* **2006**, *6*, 2225–2231.
47. Baldwin, J. A.; Vlčková, B.; Andrews, M. P.; Butler, I. S. Surface-Enhanced Raman Scattering of Mercaptopyridines and Pyrazinamide Incorporated in Silver Colloid-Adsorbate Films. *Langmuir* **1997**, *13*, 3744–3751.
48. Baldwin, J.; Schuehler, N.; Butler, I. S.; Andrews, M. P.

Integrated Optics Evanescent Wave Surface Enhanced-Raman Scattering (IO-EWSERS) of Mercaptopyridines on a Planar Optical Chemical Bench: Binding of Hydrogen and Copper Ion. *Langmuir* **1996**, *12*, 6389–6398.
49. Sun, L.; Yu, C; Irudayaraj, J. Surface-Enhanced Raman Scattering Based Nonfluorescent Probe for Multiplex DNA Detection. *Anal. Chem.* **2007**, *79*, 3981–3988.
50. Frens, G. Controlled Nucleation for the Regulation of the Particle Size in Monodisperse Gold Solution. *Nature. Phys. Sci.* **1973**, *241*, 20–22.
51. Wang, Y.; Wei, H.; Li, B.; Ren, W.; Guo, S.; Dong, S.; Wang, E. SERS Opens a New Way in Aptasensor for Protein Recognition with High Sensitivity and Selectivity. *Chem.Commun.* **2007**, *5220*, 5222.
52. Westerfield, M. The Zebrafish Book: A Guide for the Laboratory Use of Zebrafish (*Danio rerio*); University of Oregon Press: Eugene, OR, 1993; Chapters 1−4, http://zfin.org/zf_info/zfbook/zfbk.html.
53. Cole, L. K. LS Ross: Apoptosis in the Developing Zebrafish Embryo. *Dev. Biol.* **2001**, *240*, 123–42.
54. Walker, M. B.; Kimmel, C. B. A Two-Color Acid-Free Cartilage and Bone Stain for Zebrafish Larvae. *Biotech. Histochem.* **2007**, *82*, 23–8.